Photodissociation of Benzotrifluoride at 193 nm[†]

Shang-Ting Tsai,[‡] Yuan T. Lee,[§] Chi-Kung Ni*

Institute of Atomic and Molecular Science, Academia Sinica Taipei, P.O. Box 23-166, 106, Taiwan, ROC

Received: March 1, 2000; In Final Form: May 9, 2000

Photodissociation of benzotrifluoride at 193 nm was studied in molecular beam by VUV photoionization/multimass ion imaging techniques. Photofragment translational energy distributions corresponding to the F and CF_3 elimination were measured. The dissociation rate of benzotrifluoride was measured to be 6.2×10^4 s^{-1}. The experimental result indicated that the highly vibrationally excited benzotrifluoride was formed by internal conversion from an initial excited state to a ground electronic state prior to dissociation.

I. Introduction

The ultraviolet photochemistry of aromatic compounds and their related molecules has been the subject of many recent studies.[1−24] UV absorption of the phenyl halides corresponds to the excitations of electrons of the phenyl ring and the nonbonding electron of the halogen atoms. The nonbonding electron excitation of the halogen atoms leads to direct dissociation, that is, an immediate release of halogen atoms on a repulsive surface. Alternately, the excitation of the phenyl ring results in an excited state, stable with respect to dissociation. Dissociation occurs indirectly either through the coupling of the stable and repulsive state, or after the internal conversion from an initial excited state to a lower electronic state. Direct dissociation is fast and releases a large amount of kinetic energy. Indirect dissociation results in a limited release of kinetic energy due to the extensive energy randomization among vibrational degrees of freedom and has a slow dissociation rate. Direct and indirect dissociation have been observed in the photodissociation of iodobenzene,[1,2] bromobenzene,[2,3] chlorobenzene,[2,4−7] *o*-, *m*-, *p*-chlorotoluene,[7−10] benzyl chloride,[10] and *o*-, *m*-, and *p*-dichlorobenzene.[9,11,12]

The dissociation of alkyl-substituted benzenes in the UV region shows a more distinct dissociation mechanism than aryl halides. Dissociation of alkyl-substituted benzenes in the 200−250 nm region generally results in either the elimination of the H atom or C−C bond cleavage from the alkyl group. The dissociation rates are slow and kinetic energy release is small. Since the alkyl group is not an electronic chromophore in this region, the absorption corresponds to the excitation of the phenyl ring. Dissociation must be an indirect process. A reaction mechanism that proceeds through the vibrationally excited ground electronic state of alkyl-substituted benzenes, "hot molecules" were proposed to interpret the photodissociation of alkyl-substituted benzenes. The hot molecule was produced by an internal conversion from the electronically excited state, which was populated by UV absorption. The hot molecule mechanism has been observed in the dissociation of benzene,[13,14] toluene,[15−21] xylene,[20−22] trimethylbenzene,[16] tetramethylbenzene,[16] ethylbenzene,[18,19] propylbenzene,[18] and butylbenzene.[18]

In contrast to the other aryl halide compounds, the photochemistry of fluorine atom-substituted benzenes has received little attention. Since the fluorine atom is not an electronic chromophore in 200−250 nm, the dissociation mechanism in this photon energy region is similar to the alkyl-substituted benzenes. H atom elimination has been observed from the 193 nm excitation of 2,3,4,5,6-pentafluorotoluene, and a dissociation rate (an overall disappearance rate of pentafluorotoluene) of 8.5 $\times 10^5$ s^{-1} was obtained.[23] Photodissociation of benzotrifluoride at 193 nm has been previously studied.[24] CF_3 and H atom eliminations were observed, and a dissociation rate (an overall disappearance rate of benzotrifluoride) of 1.5×10^8 s^{-1} was reported. Notably, the reported lifetime of benzotrifluoride is 2−3 order of magnitude shorter than any alkyl-substituted or fluorine atom-substituted benzenes. In this paper, multimass ion imaging techniques were employed to investigate the photodissociation of benzotrifluoride at 193 nm. Photofragment translational energy distribution and dissociation rate was measured.

II. Experiment

The experiments have been described in detail elsewhere,[14,25] only a brief description is given here. The ion imaging apparatus consisted of a molecular beam, a photolysis laser beam, a VUV probe laser beam, a constant momentum mass spectrometer, and a two-dimensional ion detector. The molecular beam, photolysis laser beam, and VUV laser beam were perpendicular to each other. However, the crossing point of the photolysis laser and the molecular beam was not the same as the crossing point of the VUV laser and the molecular beam. The crossing point of the VUV laser beam and the molecular beam was fixed. The crossing point of the photolysis laser beam and the molecular beam was moveable, it was positioned 0−10 cm upstream from the crossing point of the VUV laser and the molecular beam.

Benzotrifluoride vapor was formed by flowing ultrapure He or Ar at pressures of 300 Torr through a reservoir filled with liquid benzotrifluoride at −5 °C. The benzotrifluoride/He or Ar mixture was then expanded through a 500 μm pulsed nozzle (General Valve). Benzotrifluoride molecules in the molecular beam were photodissociated by a 193 nm laser pulse. During their flight to the VUV laser beam, the fragments expanded to a larger sphere due to the recoil velocity and center-of-mass velocity. They were then ionized by the use of a VUV laser pulse. The distance and time delay between the VUV laser pulse

---

[†] Part of the special issue "C. Bradley Moore Festschrift".

[‡] Physics Department, National Taiwan University, Taipei, 106, Taiwan, ROC.

[§] Also at Chemistry Department, National Taiwan University, Taipei, 106, Taiwan, ROC.

10.1021/jp000790z CCC: $19.00

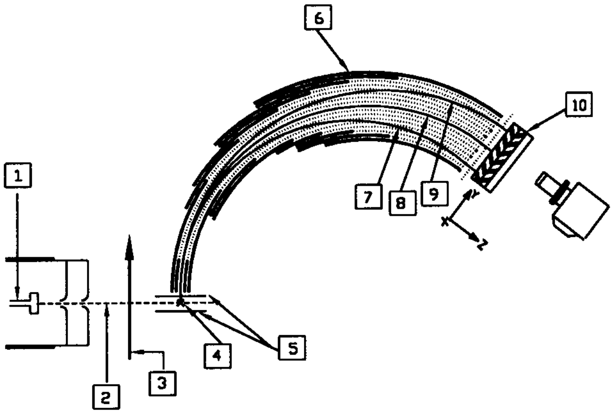

Figure 1. Schematic diagram of the multimass ion imaging detection system: (1) nozzle; (2) molecular beam; (3) photolysis laser beam; (4) VUV laser beam; (5) ion extraction plates; (6) energy analyzer; (7)−(9) simulation trajectories of $m/e = 16, 14, 12$; (10) 2D ion detector.

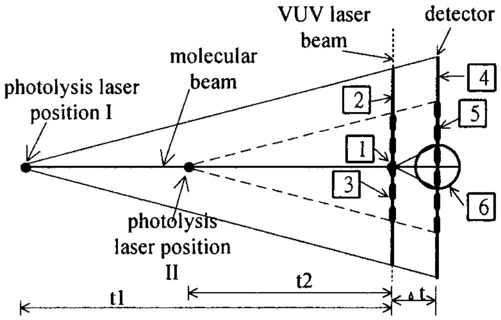

Figure 2. Relationship between the lengths of the image that resulted from different photolysis laser positions as well as the disklike image from the dissociation after ionization. (1) represents the crossing point of the molecular beam and the VUV laser beam, where the dissociative ionization (reactions 7−10) occurs. (2) and (3) represent the lengths of fragment ion segments created by the VUV laser photoionization from two different photolysis laser positions. (4) and (5) represent the lengths of the fragment ion image on the detector from two different photolysis laser positions. (6) represents the disklike image from reactions 5−12. t_1 and t_2 represent the two different delay times between the photolysis laser pulse and the VUV laser pulse. Δt is the flight time in the mass spectrometer.

and the photolysis laser pulse were set such that it ensured that the VUV laser beam passed through the center of mass of dissociation products. A segment of line of photofragment ions was generated by photoionization through the center of mass of dissociation products. The length of the segment was proportional to the fragment recoil velocity in the center-of-mass frame multiplied by the delay time between the photolysis and the ionization laser pulses. To separate the different masses within the ion segment, a pulsed electric field was used to extract the ions into a mass spectrometer after ionization. According to each fragment recoil velocity, the length of each fragment ion segment continued to expand in the original direction while the mass analysis was executed in the mass spectrometer. At the exit port of the mass spectrometer, a two-dimensional ion detector was used to detect the ion position and intensity distribution. In this two-dimensional detector, one direction was the recoil velocity axis and the other was the mass axis. The experimental schematic is illustrated in Figure 1. The recoil velocity distributions in the center-of-mass frame of various fragments were simultaneously obtained from the position and intensity distributions of the image.

According to the velocity of molecular beam, it was necessary to change the distance between the photolysis laser beam and

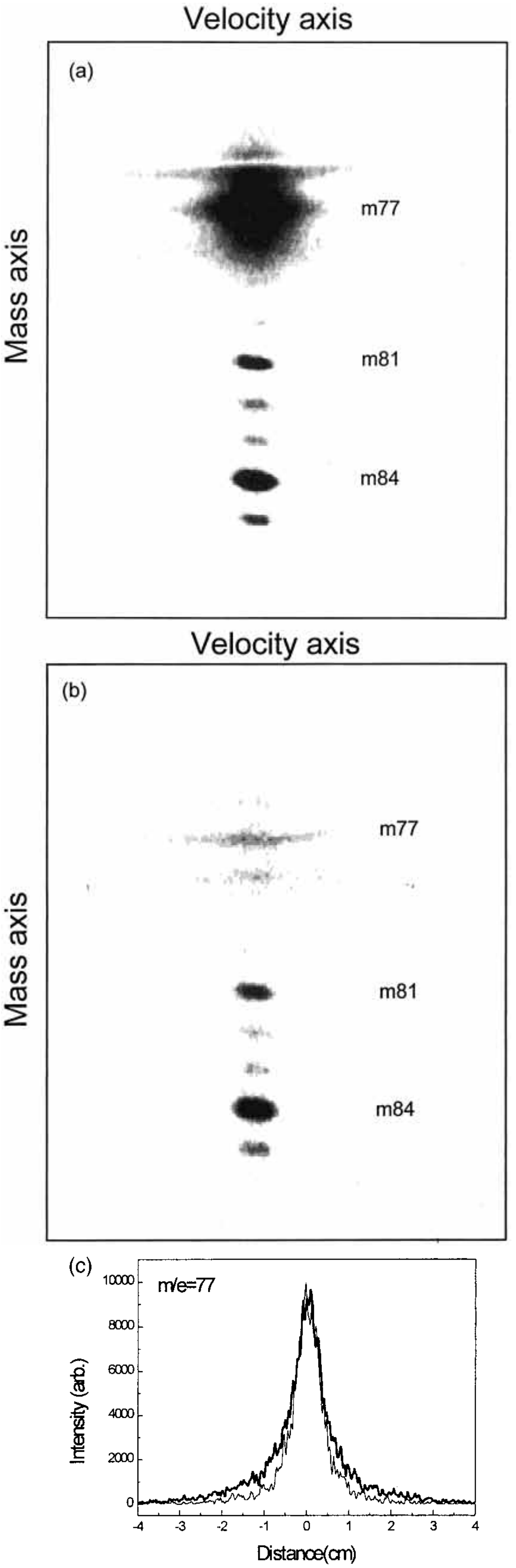

Figure 3. Image of photofragment $m/e = 77$ at (a) 78 μs and (b) 26 μs. Masses between 81 and 85 are various D atom-substituted benzenes, which are used as mass indicators. They also demonstrate the multimass detection capability. (c) The intensity profiles of image $m/e = 77$ at 78 μs (thick solid line) and 34 μs (think solid line) delay time. The intensities have been normalized for easy comparison.

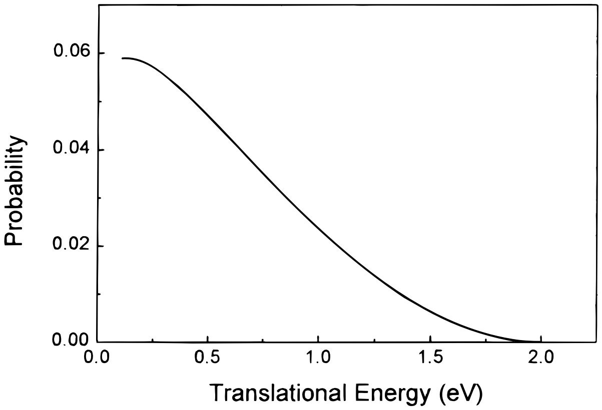

Figure 4. Translation energy distribution of the CF_3 elimination channel. Energy distribution less than 0.1 eV was obscured by disklike image and can therefore not be determined.

VUV laser beam to match the delay time between these two laser pulses to ensure that the ionization laser would pass through the center of mass of the products. The change of the distance between two laser beams also changed the length of the fragment ion segment in the image. The relationship between the length of the ion image and the position of the photolysis laser is illustrated in Figure 2.

If the molecules were not dissociated after the absorption of 193 nm photons, these high internal energy molecules would remain within the molecular beam. They fly with the same velocity (molecular beam velocity) to the ionization region and were ionized by the VUV laser. The wavelength of the VUV laser in this experiment was set at 118.2 nm, for which the photon energy was only large enough to ionize benzotrifluoride molecules. After the ionization, the energy that remains was not sufficient to result in the dissociation of benzotrifluoride cations. However, the dissociation occurred following the VUV laser ionization for those hot molecules, which absorbed 193 nm photon without dissociation. The ion image of the dissociative ionization was different from the image due to dissociation products of neutral benzotrifluoride. Since ionization and dissociation occurred at the same position, the image of dissociative ionization was a 2D projection of the photofragment ion's 3D-recoil velocity distribution. It was very similar to the image from the conventional ion imaging techniques. It was a disklike image, rather than a line shape image. As shown in Figure 2, the width of the disklike image does not change with the delay time between two laser pulses. From the shape of the image and the change in the delay time, the neutral molecule dissociation image can be easily distinguished from the dissociative ionization image.

Since the disklike image resulted from the dissociative ionization of hot molecules, the decay of the disklike image's intensity represents the decay of hot molecules. The dissociation rate (overall disappearance rate of hot parent molecules), therefore, can be obtained by measuring the intensity change of disklike image with the delay time between the pump and probe lasers.

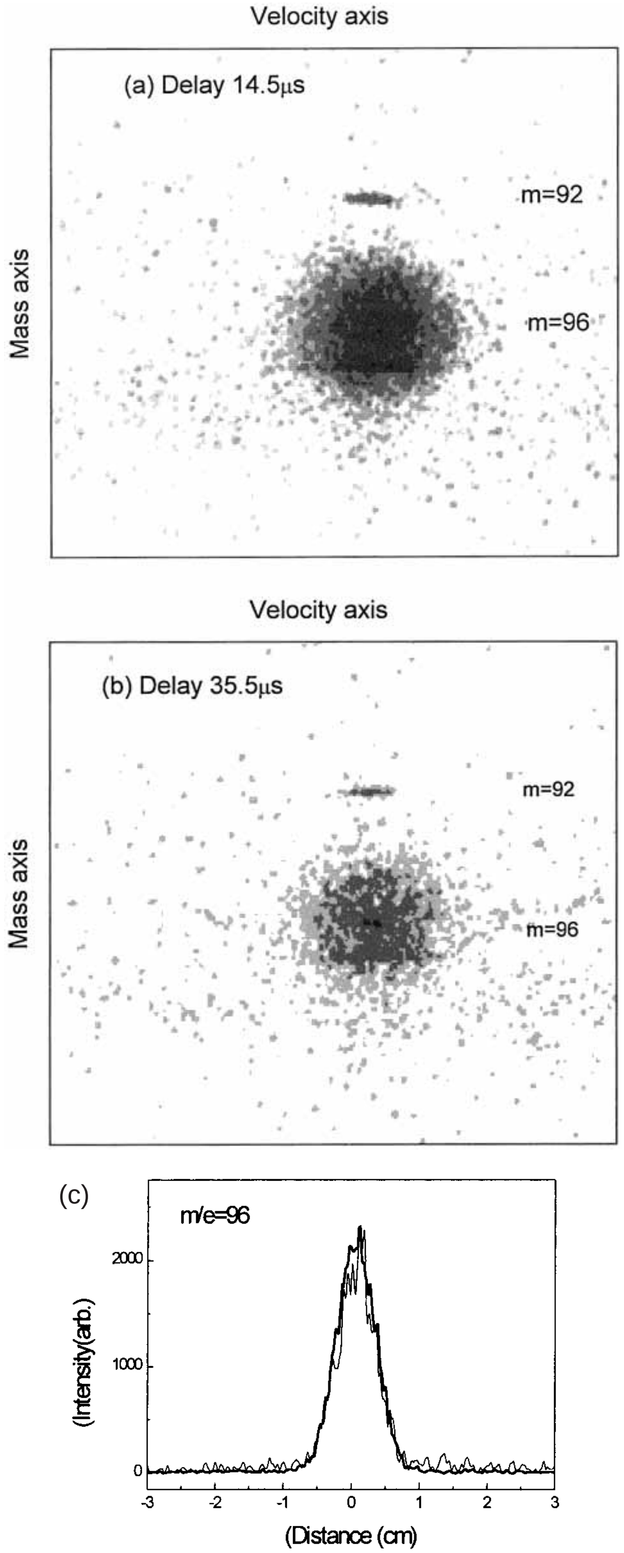

Figure 5. Image of photofragment $m/e = 96$ at (a) 14.5 μs and (b) 34.5 μs. (c) The intensity profiles of image $m/e = 96$ at delay time of 14.5 μs (thick solid line) and 34.5 μs (think solid line). The intensities have been normalized for easy comparison.

III. Results

Fragments of masses $m/e = 76, 77, 78, 96, 125, 126, 127$, and 145 were observed in the image. However, the measurements of photolysis laser power dependence in the 0.16−2 mJ/cm^2 region demonstrates that 76 and 125 masses resulted from two-photon absorption. The intensity ratio of mass 78 and 77 shows that mass 78 was due to the ^{13}C isotope of the fragment mass 77. Only the fragments that resulted from one-photon absorption will be considered herein.

Figure 3 illustrates the image of photofragment $m/e = 77$ at two different delay times. At short delay time, the image obviously consisted of two components, that is, a disklike image was superimposed on a line shape image. The disklike image resulted from the dissociative ionization of hot benzotrifluoride

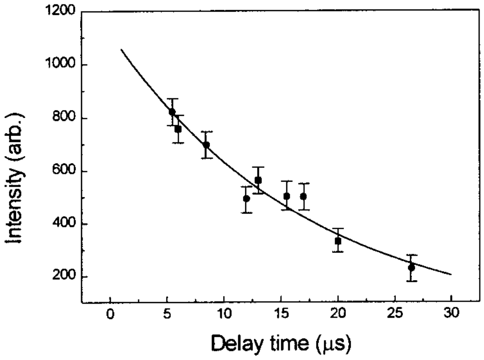

Figure 6. Intensity change of the disklike image $m/e = 96$ with the delay time. The hot benzotrifluoride dissociation rate of $6.2 \times 10^4\ s^{-1}$ was obtained from the fit of the solid line.

by the VUV laser. The line shape image was due to the photofragment from the dissociation of neutral benzotrifluoride. When the delay time between photolysis and the VUV laser pulse increased, most of the hot benzotrifluoride molecules dissociated into fragments before ionization. The disklike image became very weak, and the length of the line shape image increased. The intensity profiles of Figure 3c demonstrate that the length of the line shape image increased with the delay time. The photofragment translational energy distribution from dissociation of neutral benzotrifluoride was obtained by forward convolution of the line shape image, and the result is shown in Figure 4. The distribution of translational energy less than 0.1 eV was obscured by the disklike image and cannot be determined.

The image of mass 96 is a disklike image, with an unchanging width and shape regardless of delay time, as shown in Figure 5. This is entirely due to the dissociative ionization of hot benzotrifluoride by VUV laser. The intensity decay of the disklike image with the delay time between the UV and VUV laser pulses represents the decay of hot benzotrifluoride. The dissociation rate (overall disappearance rate) of hot benzotrifluoride, therefore, can be measured from the intensity change of mass 96 with the delay time. The intensity change of the disklike image with the delay time is shown in Figure 6. A dissociation rate of $6.2 \times 10^4\ s^{-1}$ was obtained.

The images of mass 127 and 126 show similar properties to the image of mass 77. A disklike image was superimposed on a line shape image, as shown in Figure 7a,b for two different delay time. Since the position of the images of mass 127 and 126 were very close to each other, the corresponding disklike images of these two masses partially overlapped. However, the components of the line shape image were still easily distinguished from each other. The intensity profiles in Figure 7c show that the length of the line shape image increased with the delay time. It confirms that a portion of the image resulted from the dissociation of neutral benzotrifluoride. Mass 126 has the same intensity profile as mass 127. Since the delay time between two laser pulses (34.6 and 78.6 μs) was much longer than the flight time in the mass spectrometer (7.5 μs), the identical intensity profiles of mass 127 and 126 indicate that the fragment of mass 126 resulted from the fragment cracking of mass 127 by VUV ionization. The translational energy distribution of the F atom elimination channel was obtained from the component of the line shape image and is shown in Figure 8. Figure 9 shows the intensity profile of mass 145 at two different delay times. However, there was no change in the width. Therefore, mass 145 is due to the dissociative ionization of hot benzotrifluoride by the VUV laser pulse.

IV. Discussion

The following reactions describe the results of the experiments:

$$C_6H_5CF_3 + h\nu_{193\ nm} \rightarrow C_6H_5CF_3{}^* \tag{1}$$

$$C_6H_5CF_3{}^* \rightarrow C_6H_5CF_3{}^{\ddagger} \tag{2}$$

$$C_6H_5CF_3{}^{\ddagger} \rightarrow C_6H_5CF_2 + F \tag{3}$$

$$C_6H_5CF_3{}^{\ddagger} \rightarrow C_6H_5 + CF_3 \tag{4}$$

$$C_6H_5CF_2 + h\nu_{VUV} \rightarrow C_6H_5CF_2{}^+ + e^- \text{ (or } C_6H_4CF_2{}^+ + H + e^-) \tag{5}$$

$$C_6H_5 + h\nu_{VUV} \rightarrow C_6H_5{}^+ + e^- \tag{6}$$

$$C_6H_5CF_3{}^{\ddagger} + h\nu_{VUV} \rightarrow C_6H_5F^+ + CF_2 + e^- \text{ (or } C_3H_3F_3{}^+ + C_4H_2 + e^-) \tag{7}$$

$$C_6H_5CF_3{}^{\ddagger} + h\nu_{VUV} \rightarrow C_6H_5CF_2{}^+ + F + e^- \text{ (or } C_6H_4CF_2{}^+ + H + e^-) \tag{8}$$

$$C_6H_5CF_3{}^{\ddagger} + h\nu_{VUV} \rightarrow C_6H_5{}^+ + CF_3 + e^- \tag{9}$$

$$C_6H_5CF_3{}^{\ddagger} + h\nu_{VUV} \rightarrow C_6H_4CF_3{}^+ + H + e^- \tag{10}$$

Here $C_6H_5CF_3{}^*$ represents benzotrifluoride in the second singlet electric excited state, and $C_6H_5CF_3{}^{\ddagger}$ represents the highly vibrationally excited ground state of benzotrifluoride, or hot benzotrifluoride. Reactions 3 and 4 represent the dissociation of neutral hot benzotrifluoride, and reactions 5 and 6 represent the detection of fragments by VUV laser ionization. Reactions 7−10 represent the various dissociative ionization processes of hot benzotrifluoride by a VUV photon. The dissociation rate, k, of hot benzotrifluoride, defined by the equation $d[C_6H_5CF_3{}^{\ddagger}]/dt = k[C_6H_5CF_3{}^{\ddagger}]$, is measured through the reaction 7.

The actual kinetic energy released at 193 nm was small, as presented in Figures 4 and 8. This is because the phenyl ring was strongly vibrational excited, and most of the energy remained in internal degrees of freedom. The limited release of kinetic energy corresponded to a high internal excitation of the reaction products, therefore indicating the hot molecule mechanism.

The dissociation rate of hot benzotrifluoride produced from 193 nm excitation was measured from the reaction 7, and a value of $6.2 \times 10^4\ s^{-1}$ was obtained. The dissociation rate of benzotrifluoride at room temperature after 193 nm excitation has been reported in previous research.[24] The apparent rate of the H atom fragment from the dissociation of benzotrifluoride was probed by 1 + 1 REMPI, and a dissociation rate (total disappearance rate of hot benzotrifluoride) of $1.5 \pm 1 \times 10^8\ s^{-1}$ was reported. The dissociation rate was 3 orders of magnitude faster than our measurement. We attempted to measure the intensity change of mass 96 and 145 (reactions 7 and 10) within a short delay time from 12 to 42 ns, and from 100 ns to 1 μs. However, no other dissociation rate was observed. The possible reasons for the difference are the multiphoton effect in the previous study, the angular momentum effect (one was performed at room temperature and the other was in molecular beam), or the H atom elimination channel being too small to be detected by our instrument.

TABLE 1: Dissociation Rate of Related Aromatic Molecules

	C−H bond dissociation rate				C−C bond dissociation rate			
compd	exp value (s^{-1})	E_a (kJ/mol)	T_V (K)	calc value (s^{-1})[d]	exp value (s^{-1})	E_a (kJ/mol)	T_V (K)	calc value (s^{-1})[d]
toluene	2×10^6[a]	374	2782	2×10^6	5×10^5[a]	436	2782	5×10^5
pentafluorotoluene	8.7×10^5[b]	374	2550	5×10^5				
xylene	3×10^5[c]	374	2390	1.4×10^5	5×10^4[c]	436	2390	2.5×10^4
benzetrifluoride					5.9×10^4[e]	450	2656	1×10^5

[a] Calculated from the overall parent molecule disappearance rate measured in refs 15, 16, and 18, and the branching ratio measured in ref 19. [b] From ref 23. [c] Calculated from the overall parent molecule disappearance rate measured in ref 23 and the branching ratio measured in ref 22. [d] Calculated from eq 12 and normalized to toluene dissociation rate constant. [e] From this work.

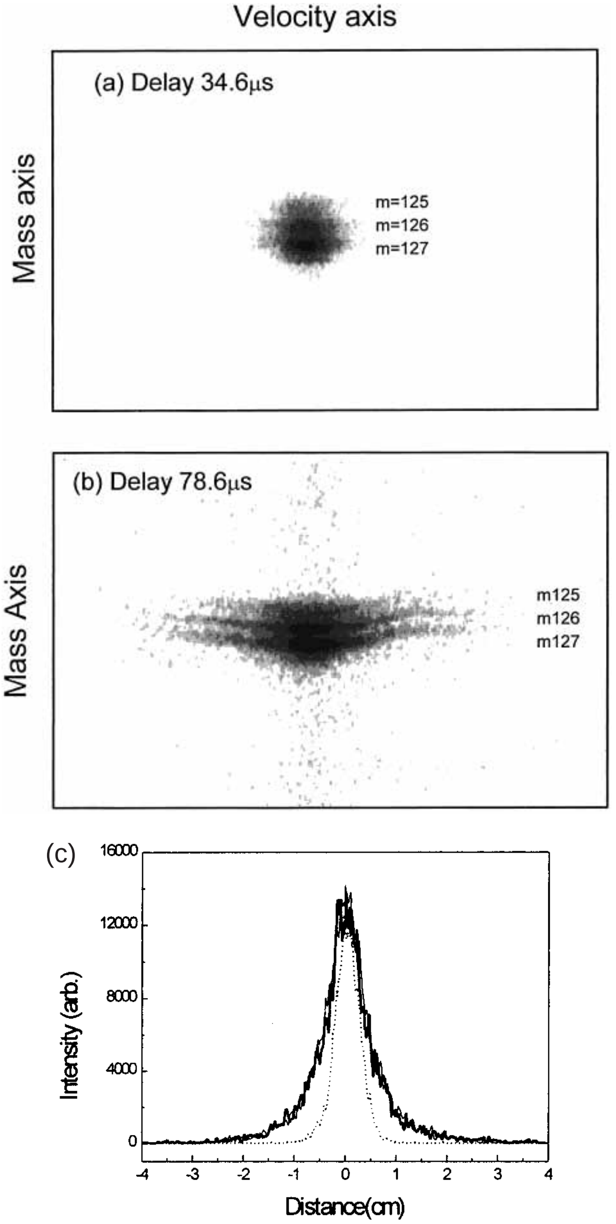

Figure 7. Image of photofragment $m/e = 127$ at delay times of (a) 34.6 μs and (b) 78.6 μs. (c) The intensity profiles of image $m/e = 127$ at delay times of 85 μs (thick solid line) and 36 μs (think dot line). The intensity profile of image $m/e = 126$ at a delay time of 85 μs (think solid line) completely overlapped with the $m/e = 127$ profile at the same delay time. The intensities have been normalized for easy comparison.

The dissociation rates of many aromatic compounds have been measured by various methods. Table 1 displays several of the aromatic molecule dissociation rates. The molecules listed in Table 1 are dissociated through the hot molecule mechanism.

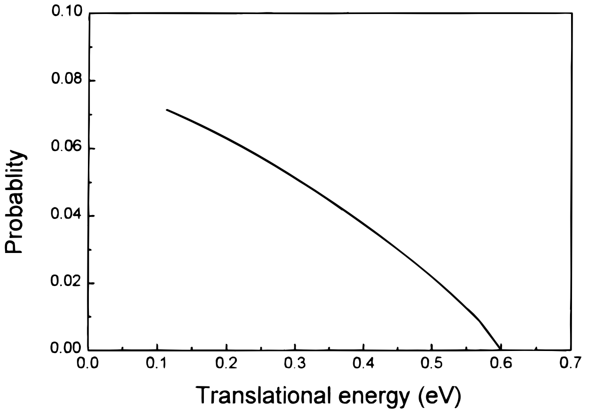

Figure 8. Translation energy distribution of the F elimination channel. Energy distributions less than 0.12 eV were obscured by a disklike image and cannot be determined.

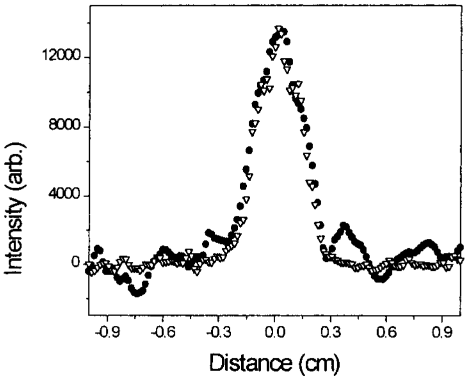

Figure 9. Intensity profiles of mass 145 at delay times of 20.5 and 46.5 μs.

Dissociation rates calculated by the RRKM method generally agree with the experimental results. Another simple model proposed by Bersohn can estimate the dissociation rate of these hot aromatic molecules.[16,23] The model assumes that after the aromatic molecule absorbs a relatively high energy photon, rapid internal conversion occurs and the isolated molecule can then be presumed to have an internal vibrational temperature T_v. This was determined by solving the equation

$$E + \sum_i \hbar\omega_i/[\exp(\hbar\omega_i/kT) - 1] = \sum_i \hbar\omega_i/[\exp(\hbar\omega_i/kT_v) - 1] \tag{11}$$

where E is the photon energy, T is the molecular beam vibrational temperature, and ω_i is the vibrational frequency of the molecules. The equation states that the photon energy plus the initial vibrational energy is equal to the energy that is distributed throughout the molecule with a vibrational temperature T_v. The validity of this parameter depends on the facts that the photon energy supplied is larger than any vibrational quantum of the molecules and the number of vibrational modes is large. If we assume that the activation energy is the bond energy of these barrierless dissociation channels, then the decomposition rate constant $k(E)$ can be expressed as follows:

$$k(E) = A \exp(-E_a/kT\upsilon) \tag{12}$$

Although the calculation is crude, it does provide the concept and the trend of the dissociation rates between the various molecules. It has been applied in many aromatic compounds and produces reasonable results.[16,23] Table 1 lists the decomposition rates of various molecules in two types of decomposition. One is the C−H bond dissociation rate, and the other is the C−C bond dissociation rate. If we assume that different molecules decompose with the same *A* factor in each type of chemical bond cleavage, the ratio of dissociation rate between various molecules can therefore be obtained from eq 12. Calculated results of various molecules obtained from eq 12 are normalized to the dissociation rate of toluene and are listed in Table 1. The agreement between the experimental value and the calculated result was very good. A comparison of benzotrifluoride experimental and calculated results suggested that the dissociation lifetime of benzotrifluoride be in the microsecond region.

In conclusion, the F atom and CF_3 eliminations from the benzotrifluoride after 193 nm excitation have been observed. The translational energy distribution of the photofragments and the dissociation rate were measured by the multimass ion imaging technique. The dissociation rate and the translational energy distribution suggested that the dissociation occurred from the highly vibrationally excited ground state after the internal conversion from an initially excited state. Interestingly, this new technique not only can simultaneously measure translational spectroscopy of various photofragments but also can distinguish the channels between neutral molecule dissociation (reactions 3 and 4) and dissociative ionization (reactions 7−10). These two capabilities cannot be achieved by conventional ion imaging techniques.

Acknowledgment. The authors thank the National Science Council of the Republic of China for financially supporting this research under Contract No. NSC 89-2113-M-001-028.

References and Notes

(1) Dzvonik, M.; Yang, S.; Bersohn, R. *J. Chem. Phys.* **1974**, *61*, 4408.

(2) Freedom, A.; Yang, S. C.; Kawasaki, M.; Bersohn, R. *J. Chem. Phys.* **1980**, *72*, 1028.

(3) Zhang, H.; Zhu, R. S.; Wang, G. J.; Han, K. L.; He, G. Z.; Lou, N. Q. *J. Chem. Phys.* **1999**, *110*, 2922.

(4) Han, K. L.; He, G. Z.; Lou, N. Q. *Chem. Phys. Lett.* **1993**, *203*, 509.

(5) Wang, G. J.; Zhu, R. S.; Zhang, H.; Han, K. L.; He, G. Z.; Lou, N. Q. *Chem. Phys. Lett.* **1998**, *288*, 429.

(6) Ichimura, T.; Mori, Y.; Shinohara, H.; Nishi, N. *Chem. Phys.* **1994**, *189*, 117.

(7) Ichimura, T.; Mori, Y.; Shinohara, H.; Nishi, N. *Chem. Phys. Lett.* **1985**, *122*, 51.

(8) Kawasaki, M.; Kasatani, K.; Sato, H.; Shinohara, H.; Nishi, N. *Chem. Phys.* **1984**, *88*, 135.

(9) Ichimura, T.; Mori, Y.; Shinohara, H.; Nishi, N. *J. Chem. Phys.* **1997**, *107*, 835.

(10) Satyapal, S.; Tasaki, S.; Bersohn, R. *Chem. Phys. Lett.* **1993**, *203*, 349.

(11) Zhu, R. S.; Zhang, H.; Wang, G. J.; Gu, X.; Han, K. L.; He, G. Z.; Lou, N. Q. *Chem. Phys.* **1999**, *248*, 285.

(12) Ichimura, T.; Shimoda, A,; Kikuchi, T.; Kohso, Y.; Hikid, T.; Mori, Y. *J. Photochem.* **1985**, *31*, 157.

(13) Yokoyama, A.; Zhao, X.; Hintsa, E. J.; Continetti, R. E.; Lee, Y. T. *J. Chem. Phys.* **1990**, *92*, 4222.

(14) Tsai, Shang-Ting; Lin, Chih-Kai; Lee, Yuan, T.; Ni, Chi-Kung. Dissociation rate of hot benzene. *J. Chem. Phys.*, in press.

(15) Hipper, H.; Schubert, V.; Troe, J.; Wendelken, H. J. *Chem. Phys. Lett.* **1981**, *84*, 253.

(16) Park, J.; Bersohn, R.; Oref, I. *J. Chem. Phys.* **1990**, *93*, 5700.

(17) Fröchtenicht, R. *J. Chem. Phys.* **1994**, *102*, 4850.

(18) Nakashima, N.; Yoshihara, K. *J. Phys. Chem.* **1989**, *93*, 7763.

(19) Luther, K.; Troe, J.; Weitzel, K. L. *J. Phys. Chem.* **1990**, *94*, 6316.

(20) Brand, U.; Hippler, H.; Lindemann, L.; Troe, J. *J. Phys. Chem.* **1990**, *94*, 6305.

(21) Shimada, T.; Ojima, Y.; Nakashima, N.; Izawa, Y.; Yamanaka, C. *J. Phys. Chem.* **1992**, *96*, 6298.

(22) Lange, S.; Luther, K.; Rech, T.; Schmoltner, A. M.; Troe, J. *J. Phys. Chem.* **1994**, *98*, 6509.

(23) Min, Z.; Wong, T. H.; Bersohn, R. *J. Chem. Phys.* **1999**, *110*, 9956.

(24) Fröchtenicht, R.; Hartmann, M. *Chem. Phys. Lett.* **1996**, *250*, 209.

(25) Tsai, Shang-Ting; Lin, Chih-Kai; Lee, Yuan, T.; Ni, Chi-Kung. Multimass ion imaging detection of photofragment translational spectroscopy. Submitted to *Rev. Sci. Instrum.*